2002

Synthesis of Layered-Structure LiMn1−xCrxO2 by the Pechini Method

Z. P. Guo
University of Wollongong, zguo@uow.edu.au

S. Zhong
University of Wollongong

G. X. Wang
University of Wollongong, gwang@uow.edu.au

G. W. Walter
University of Wollongong

Hua-Kun Liu
University of Wollongong, hua@uow.edu.au

See next page for additional authors

Journal of The Electrochemical Society, **149** (6) A792-A795 (2002)
0013-4651/2002/149(6)/A792/4/$7.00 © The Electrochemical Society, Inc.

Synthesis of Layered-Structure $LiMn_{1-x}Cr_xO_2$ by the Pechini Method and Characterization as a Cathode for Rechargeable Li/$LiMnO_2$ Cells

Z. P. Guo,[z] S. Zhong, G. X. Wang,* G. Walter, H. K. Liu, and S. X. Dou**

Institute for Superconducting and Electronic Materials, University of Wollongong, NSW 2522, Australia

$LiMn_{1-x}Cr_xO_2$ compounds with an α-$NaFeO_2$ layer-type crystal structure have been prepared by the Pechini method. The effects of ethylene glycol (EG) content and calcination temperature on powder characteristics and electrochemical performance are evaluated. It is found that the homogeneity of the powder is increased by increasing the molar ratio of EG to citric acid, and a trace of MnO can be detected in the powder calcined below 800°C for 4 h. Compared with the ss-$LiMn_{1-x}Cr_xO_2$ powder (made by the solid-state reaction), the p-$LiMn_{1-x}Cr_xO_2$ compound (made by the Pechini method) yielded higher specific capacity for both charge and discharge, and the rate capability has been improved due to the smaller particle size and good homogeneity. The evolution of discharge curves with cycling shows that less additional spinel-type tetrahedral sites for Li formed during cycling of the p-$LiMn_{1-x}Cr_xO_2$ compound.
 [DOI: 10.1149/1.1477206]

Manuscript received November 14, 2001. Available electronically April 30, 2002.

Lithium manganese oxides have been investigated as low-cost positive electrode materials in rechargeable lithium-ion batteries. In particular, cation-doped/undoped $LiMn_2O_4$ positive electrode materials have been examined extensively.[1-3] A trivalent manganese compound, $LiMnO_2$, is also a candidate for a positive electrode for lower cost and higher capacity lithium-ion batteries. $LiMnO_2$, obtained by solid-state reaction, tends to have a corrugated layer structure,[4] (*Pmnm*, *ortho*-$LiMnO_2$), instead of a layered rock salt structure, like $LiCoO_2$ and $LiNiO_2$. The structure changes easily to the spinel-related form during electrochemical cycling of a Li/*ortho*-$LiMnO_2$ cell between 2.0 and 4.4 V.[5-8] The presence of two different plateaus at 3 and 4 V in the charge/discharge curves is not suitable from a practical point of view. Recently, metastable $LiMnO_2$ with a layered rock salt structure (layered structure) was synthesized from α-$NaMnO_2$ by an ion-exchange method,[9-11] or directly from a solid-state reaction with Cr or Al doping.[12,13] The charge capacity of a Li/$LiMnO_2$ cell is as high as 280 mAh/g up to 4.4 V, and would be important for practical considerations.

When scaling-up for commercialization, both the ion-exchange method and solid-state reaction take a long time and use excessive lithium.[14] The Pechini process[15] can, within several hours, produce a capacity above 160 mAh/g (room temperature, 50 mA/g) together with excellent cycling behavior.

In this work, layered $LiMn_{1-x}Cr_xO_2$ powder has been synthesized by the Pechini method. Since lithium evaporation could occur during the synthesis, excessive lithium [Li/(Mn + Cr) = 1.1] is used to maintain stoichiometry. The characteristics and electrochemical performance of samples obtained were investigated, and were compared with that of layered-$LiMn_{1-x}Cr_xO_2$ prepared by a solid-state reaction. In order to clearly show the comparison of results, the data relative only to $LiMn_{0.9}Cr_{0.1}O_2$ composite are given in the present paper.

Experimental

Powder preparation.—Reagents of $MnCO_3$ (Aldrich Chemicals, 99%), $Cr(NO_3)_3 \cdot 9H_2O$ (Aldrich Chemicals, 99%), Li_2CO_3 (Aldrich Chemicals, 99.99%), citric acid (CA, Aldrich Chemicals, 99.5%), ethylene glycol (EG, Aldrich Chemicals, extra pure), and nitric acid (Aldrich Chemicals, 60%) were used as starting materials. $MnCO_3$ and $Cr(NO_3)_3 \cdot 9H_2O$ were dissolved in diluted nitric acid with several drops of hydrogen peroxide until a clear solution was obtained. Stoichiometric amounts of Li_2CO_3 were then added to the solution.

Predissolved solutions of CA and EG with a molar ratio (R) for EG to CA of 1, 2, and 4 were added to the clear (completely soluble) cation solutions. These mixed solutions were stirred on a hot plate, which allowed the temperature to be controlled below 180°C, until the solutions became a dark-green gel. This was followed by drying in a vacuum to evaporate the residual water (from 120 to 170°C, step-by-step) and, finally, a puffed char (a voluminous sponge), was obtained. The puffed precursors were transferred to crucibles and were calcined in a tube furnace at 600, 700, and 800°C for 4 h under the flow of argon.

Phase analysis was carried out by powder X-ray diffraction (XRD) with Cu Kα radiation in a 1730 X-ray diffractometer. Scanning electron micrographs (SEM) were obtained to examine the morphology of the powder.

Electrochemical measurements.—A cathode was prepared by mixing $LiMn_{0.9}Cr_{0.1}O_2$ powder with 10 wt % carbon black and 5 wt % polyvinylidene fluoride (PVDF) solution. The $LiMn_{0.9}Cr_{0.1}O_2$ and carbon black powders were first added to a solution of PVDF in *N*-methyl-2-pyrrolidinone (NMP) to make a slurry with appropriate viscosity. Al foil was then used to coat the mixture. After the electrode was dried at 140°C for 2 h in vacuum, it was compressed at a rate of about 150 kg/cm^2. Teflon test cells were assembled in an argon-filled glove box, where the counter electrode was Li metal and the electrolyte was 1 M $LiPF_6$ dissolved in a 50/50 vol % mixture of ethylene carbonate (EC) and dimethyl carbonate (DMC). These cells were cycled between 2.0 and 4.4 V at room temperature to measure the electrochemical response. In order to measure the electrochemical impedance response, an EG&G model 6310 electrochemical impedance analyzer was used, and electrochemical impedance software (model 398) was used to control a computer for conductivity and stability measurements. After the electrode attained a steady-state potential, electrochemical impedance measurements were carried out by applying an ac voltage of 5 mV over the frequency range from 1 mHz to 100 kHz.

Results and Discussion

Preparation of powders.—During evaporation of the water from the mixed solution, precipitates of the polymer, which have a light-gray color, were observed with a small addition of EG (R = 1). The vacuum-dried precursors took the form of a sponge-like dark-green char. The apparent volume of the precursor increased with an increase in the EG to CA ratio. An optimal gelling condition is achieved at a ratio of EG to CA of 4:1. Tai and Lessing[16] have

* Electrochemical Society Active Member.
** Electrochemical Society Student Member.
[z] E-mail: zgo4@uow.edu.au

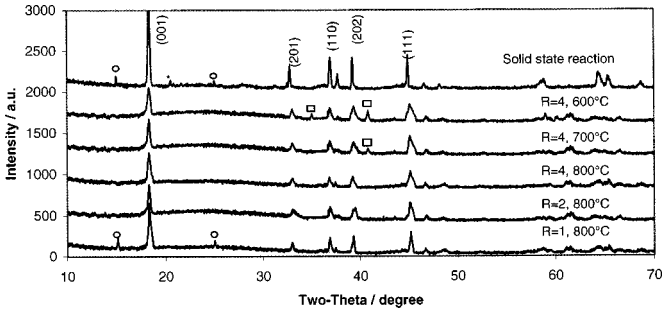

Figure 1. XRD patterns of p-$LiMn_{0.9}Cr_{0.1}O_2$ and ss-$LiMn_{0.9}Cr_{0.1}O_2$ materials [Li/(Mn + Cr) = 1.1 in precursor and ss-$LiMn_{0.9}Cr_{0.1}O_2$ material calcined at 1000°C for 10 h]. (○) $LiMnO_2$ (*ortho*); (□) MnO; (*) Li_2MnO_3.

reported that an optimal gelling condition is achieved near a ratio of EG to CA of 1:1, and the resultant resins had the largest apparent volumes among the samples. The reason why our experiment was not consistent with the condition proposed by Tai and Lessing is thought to be due to the fact that sufficient reaction could not occur because the polymerization could only take place for several hours during the drying process. The XRD patterns of $LiMn_{0.9}Cr_{0.1}O_2$ samples prepared at various R ratios are given in Fig. 1. The main peaks for the layered (monoclinic) phase are labeled with their *hkl* indexes. Positions for peaks characteristic of orthorhombic *o*-$LiMnO_2$ phase, MnO and Li_2MnO_3, are indicated, respectively. Compared with the $LiMn_{0.9}Cr_{0.1}O_2$ prepared by solid-state reaction with Li/(Mn + Cr) = 1.1 calcined at 1000°C for 10 h, the XRD peaks of $LiMn_{0.9}Cr_{0.1}O_2$ by the Pechini method broadened remarkably, and the extent of broadening is larger for $R = 2$, 4 than for $R = 1$. Orthorhombic *o*-$LiMnO_2$ phase was observed in XRD patterns for the solid-state reaction sample, with a small addition of EG ($R = 1$) sample. The reason for this may be that the Cr cation distribution in precursors is not as uniform as that in high R ($R = 2, 4$) samples. When sintering, part of the powder is not doped by Cr, which leads to a small amount of *o*-$LiMnO_2$ being produced.

Unit cell parameters for the monoclinic-layered $LiMn_{0.9}Cr_{0.1}O_2$ phases are reported in Table I. Compared with the $LiMn_{0.9}Cr_{0.1}O_2$ compound prepared by solid-state reaction, the $LiMn_{0.9}Cr_{0.1}O_2$ here shows contracted crystal lattices. In the *ab* plane, the contraction is more significant along the *a* axis than the *b* axis. The extent of monoclinic distortion is reflected in the magnitude of the a/b ratio and is related to the average degree of distortion of the octahedron for oxygen ions around the cations in the Mn layer. Therefore, a greater contraction along the *a* axis may associate with more uniform Cr substitution in $LiMnO_2$ compounds. The powder prepared with a large amount of EG is close to the optimal gelling conditions in which there is a more extended three-dimensional network, *i.e.*, more homogeneous mixing of the cation, and less tendency for segregation during sintering. Therefore, it is found that increasing R increases the homogeneity of the sample.

The final morphologies of the calcined powders are given in Fig. 2. It is clear that the particle size decreases with increasing R. With

Table I. Monoclinic unit cell parameters for $LiMn_{0.9}Cr_{0.1}O_2$ materials sintering at 800°C with different R ratios (R = molar ratio of EG to CA).

	a (Å)	*b* (Å)	*c* (Å)	β
$R = 4$	5.379	2.825	5.354	115.09°
$R = 2$	5.384	2.825	5.361	115.16°
$R = 1$	5.391	2.821	5.369	115.30°
Sample by solid-state reaction	5.406	2.813	5.378	115.72°

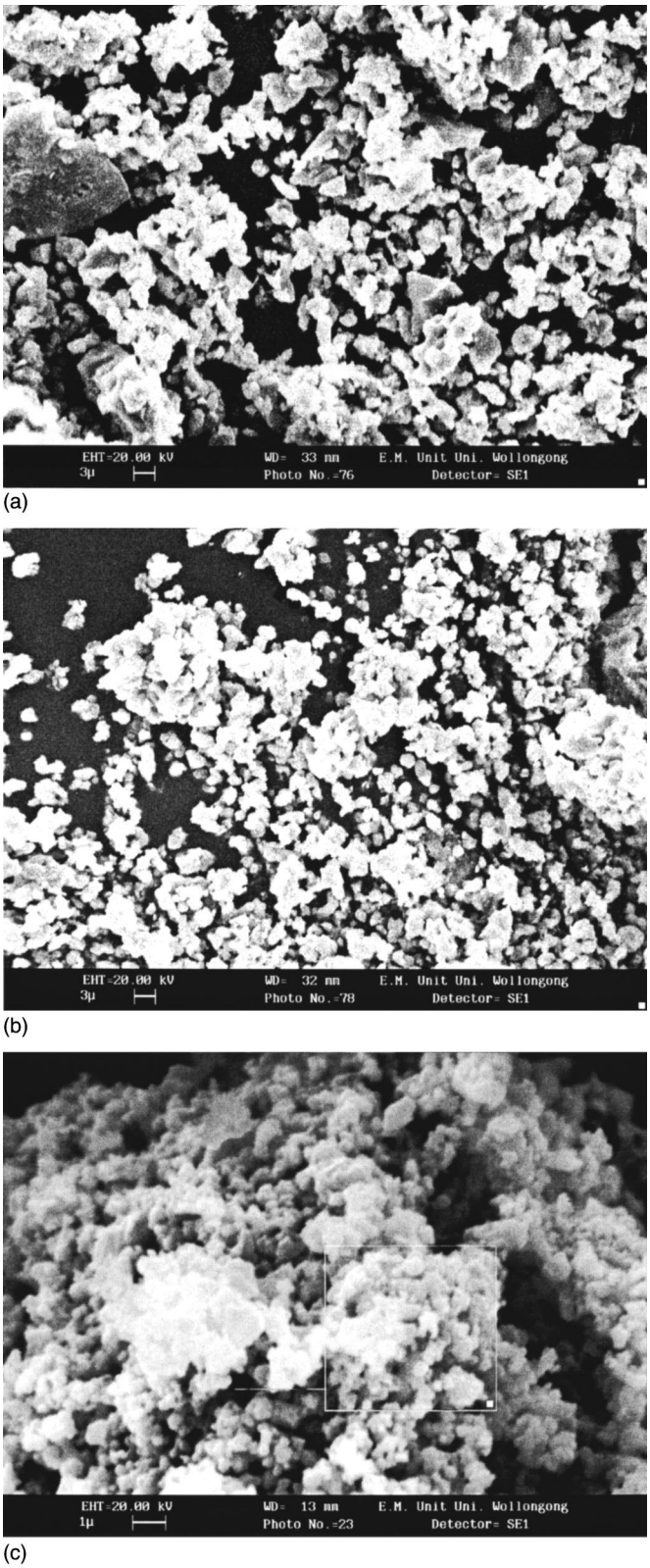

Figure 2. (a, top) Electron micrographs of calcined powder at 800°C for 4 h from the solution with $R = 1$ (R = molar ratio of EG to CA). (b, center) Electron micrographs of calcined powder at 800°C for 4 h from the solution with $R = 2$. (c, bottom) Electron micrographs of calcined powder at 800°C for 4 h from the solution with $R = 4$.

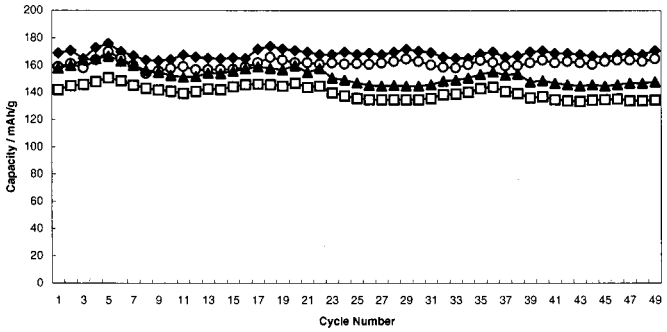

Figure 3. Cycling data at room temperature for Li cells containing ss-$LiMn_{0.9}Cr_{0.1}O_2$ and p-$LiMn_{0.9}Cr_{0.1}O_2$. (♦) p-$LiMn_{0.9}Cr_{0.1}O_2$, charge; (○) p-$LiMn_{0.9}Cr_{0.1}O_2$, discharge; (▲) ss-$LiMn_{0.9}Cr_{0.1}O_2$, charge; (□) ss-$LiMn_{0.9}Cr_{0.1}O_2$, discharge. (Current rate 50 mA/g, room temperature.)

a small addition of EG ($R = 1$), there are abnormally coarsened particles. As mentioned above, the drying of solutions for $R = 1$ produces precipitates. Monchilov *et al.*[17] have reported that manganese oxide has a considerably greater tendency for crystal growth by a solid-state reaction than lithium manganese oxide. Therefore, the abnormally coarsened particles can be partly explained by the Mn-rich phase promoting the growth of particles.

The effect of sintering temperature on the characteristics of samples was also investigated. The XRD patterns of calcined powder at different temperatures are presented in Fig. 1. When the sample was fired at 600°C, a large amount of MnO was produced. A trace of MnO is also detected in the powder calcined at 700°C for 4 h.

Based on the discussion above, it can be concluded that the optimum R and sintering temperature for $LiMn_{0.9}Cr_{0.1}O_2$ materials by the Pechini method are $R = 4$ and 800°C, respectively.

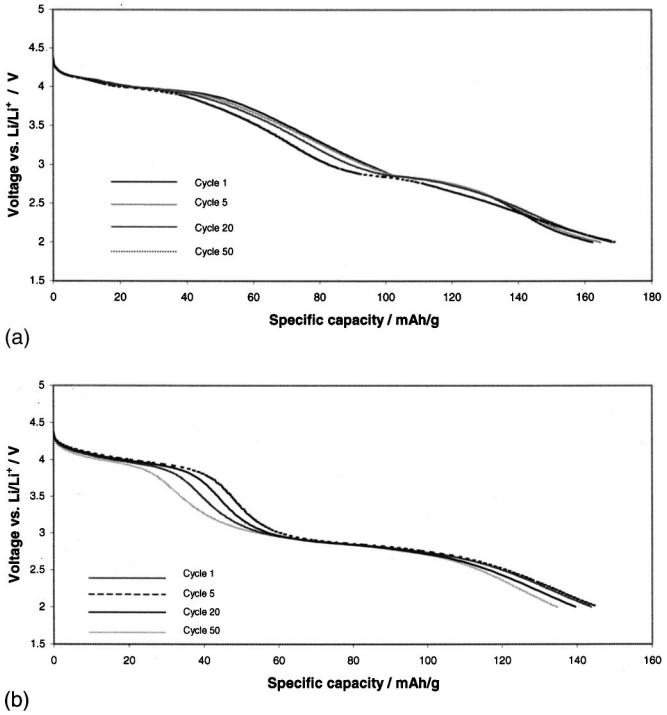

Figure 4. (a, top) Discharge curves for Li cells containing p-$LiMn_{0.9}Cr_{0.1}O_2$ at cycles 1, 5, 20, and 50 (current rate 50 mA/g, room temperature). (b, bottom) Discharge curves for Li cells containing ss-$LiMn_{0.9}Cr_{0.1}O_2$ at cycles 1, 5, 20, and 50 (current rate 50 mA/g, room temperature).

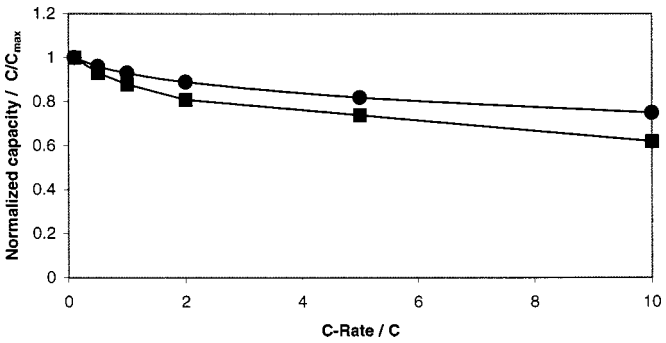

Figure 5. Changes of normalized discharge capacity (C/C_{max}) for the cells with active electrodes of (■) ss-$LiMn_{0.9}Cr_{0.1}O_2$ and (●) p-$LiMn_{0.9}Cr_{0.1}O_2$ at room temperature with a varying charge-discharge rate (0.1-10 C).

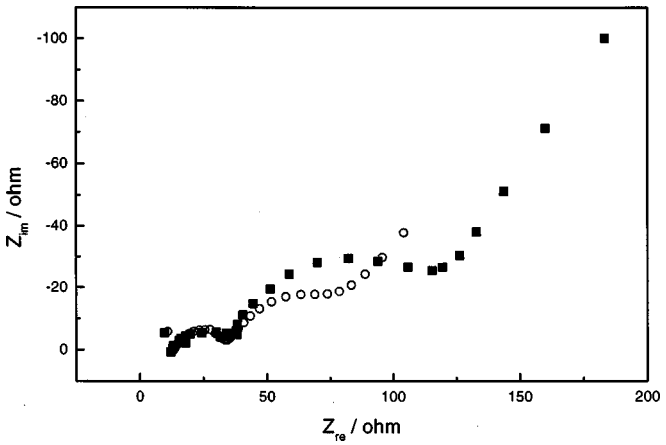

Figure 6. EIS spectra (Nyquist complex plane plots), for the cells with active electrodes of (■) ss-$LiMn_{0.9}Cr_{0.1}O_2$ and (○) p-$LiMn_{0.9}Cr_{0.1}O_2$ after five cycles at room temperature.

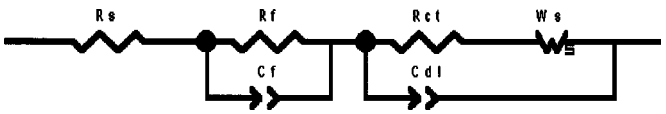

Figure 7. Equivalent circuit for the $LiMn_{0.9}Cr_{0.1}O_2$ electrode.

Electrochemical characterization.—Teflon cells, comprising layered monoclinic $LiMn_{0.9}Cr_{0.1}O_2$ materials, were cycled at ambient temperature. The corresponding charge/discharge capacities as a function of cycle number are shown in Fig. 3. Cells were charged/discharged at a current rate of 50 mA/g. It was found that the capacities of samples synthesized by the Pechini method for (p-$LiMn_{0.9}Cr_{0.1}O_2$) are ~12% higher than those obtained by solid-state reaction for (ss-$LiMn_{0.9}Cr_{0.1}O_2$), and the capacity retention at room temperature is high (>90%) for both materials.

Although both p-$LiMn_{0.9}Cr_{0.1}O_2$ and ss-$LiMn_{0.9}Cr_{0.1}O_2$ compounds show remarkable cycling stability even at room temperature, significant differences were observed in the voltage profiles. Figure 4 compares discharge curves at different cycle numbers for the cells containing p-$LiMn_{0.9}Cr_{0.1}O_2$ (Fig. 4a) and ss-$LiMn_{0.9}Cr_{0.1}O_2$ (Fig. 4b). For ss-$LiMn_{0.9}Cr_{0.1}O_2$, the first discharge is characterized by three parts between 4.4 and 2 V, *i.e.*, plateaus at 4 and 2.8 V and a relatively featureless sloping profile between 4 and 2.8 V. With continued cycling, the first plateau of discharge (4 V) evolves to a higher potential first, then drops to a lower potential. The second plateau of discharge (2.8 V) is relatively stable. This profile strongly

Table II. Results of ac impedance analysis of the ss-$LiMn_{0.9}Cr_{0.1}O_2$ and p-$LiMn_{0.9}Cr_{0.1}O_2$ compounds.

Compounds	R_s	C_f ($\times 10^{-5}$)	R_f	R_{ct}	W_s-T	C_{dl} ($\times 10^{-3}$)
p-$LiMn_{0.9}Cr_{0.1}O_2$	12.28	24.46	23.56	38.63	536.7	9.91
ss-$LiMn_{0.9}Cr_{0.1}O_2$	13.12	2.682	22.21	80.21	16.28	1.51

resembles that observed for a spinel-type manganese oxide structure, where the 4 V plateau relates to insertion of Li into tetrahedral sites, and the 2.8 V plateau relates to insertion into octahedral sites. Therefore, the data for ss-$LiMn_{0.9}Cr_{0.1}O_2$ material are consistent with recent structural analyses showing that this compound transforms to a spinel-related structure during cycling.[12]

The discharge curves for the p-$LiMn_{0.9}Cr_{0.1}O_2$ material also show an evolution with cycling, but the evolution is different from that observed for ss-$LiMn_{0.9}Cr_{0.1}O_2$ material. On the first discharge, the discharge profile shows two distinct plateaus at around 4 and 2.8 V, with a sharp drop between the two plateaus, which is similar to that for the ss-$LiMn_{0.9}Cr_{0.1}O_2$. But on subsequent cycles, the length of both the first and second plateaus of discharge (at 2.8 and 4 V) is variable, the length of the first plateau decreases, and the voltage evolves to a lower potential, while the length of the second one shows a slight increase.

Comparing Fig. 4a with b, the most important observation is that no significant additional capacity is evolved at 4 V beyond the first cycle, even after 50 cycles, indicating little or no formation of additional spinel-type tetrahedral sites for Li with cycling.[13] That means layered structure ss-$LiMn_{0.9}Cr_{0.1}O_2$ material is easier to be transformed to a spinel-related structure than p-$LiMn_{0.9}Cr_{0.1}O_2$ material during cycling.

Figure 5 compares the rate capability of p-$LiMn_{0.9}Cr_{0.1}O_2$ with that of ss-$LiMn_{0.9}Cr_{0.1}O_2$. For example, a 0.5 C rate on the *x* axis means the rate at which 50% of the extractable Li is deintercalated for 1 h when the electrode is charged up to 4.4 V. Compared with ss-$LiMn_{0.9}Cr_{0.1}O_2$, the rate capability of p-$LiMn_{0.9}Cr_{0.1}O_2$ is significantly improved. To analyze this result, EIS experiments were performed on both samples. The thickness of electrodes was controlled at 50 μm, and the coated area of the electrodes at 0.9 cm^2. Samples were initially cycled five times at room temperature, and EIS measurements were carried out after electrodes were charged up to 4.4 V. A comparison of the EIS Nyquist complex plane plots (Fig. 6) shows that the ss-$LiMn_{0.9}Cr_{0.1}O_2$ compound exhibits larger second semicircles in relation to p-$LiMn_{0.9}Cr_{0.1}O_2$, while the first semicircular arc is similar. Generally, for the cathode of the lithium ion battery, the first arc is related to the passivation film on the surface and the second arc might contain a contribution due to the compaction of particles in the composite cathode, *i.e.*, the interparticle contacts such as oxide-oxide, carbon-oxide, and carbon-carbon contacts. Therefore, the reduction in the diameter of the second arc in p-$LiMn_{0.9}Cr_{0.1}O_2$ probably can be ascribed to a decrease in the interparticle contact resistance. ZView 3C software was used to quantitatively analyze the condition of the cathode. The situation at the $LiMn_{0.9}Cr_{0.1}O_2$ electrode can be approximately represented by the equivalent circuit in Fig. 7. R_s is the solution resistance of the cell, C_f and R_f are the capacitance and resistance of the passive film, C_{dl} represents the double-layer capacitance, R_{ct} is the cathode charge-transfer resistance, W_s is a short-circuited Warburg diffusion impedance, the W_s-T value represents the Warburg coefficient, which is related to the diffusion coefficient of the lithium ions into the cathode by the formula W_s-$T = L^2/D$. L is the effective diffusion thickness, and D is the effective diffusion coefficient of the lithium ions. C_f and C_{dl} were simulated by constant-phase elements (CPEs) rather than true capacitances, to take into account the skewed, (depressed), nature of the high and low frequency semicircles. Table II lists the results of the curve fit calculated from the ac impedance data in Fig. 6, based on the equivalent circuit shown in Fig. 7. It is obvious that the p-$LiMn_{0.9}Cr_{0.1}O_2$ compound has a lower charge-transfer resistance and a larger W_s-T that may suggest that the lithium ions diffuse more easily into the p-$LiMn_{0.9}Cr_{0.1}O_2$ cathode compared to the ss-$LiMn_{0.9}Cr_{0.1}O_2$ cathode. All of these can be explained by the smaller particle size and good homogeneity of p-$LiMn_{0.9}Cr_{0.1}O_2$. Smaller particle size can increase the Li^+ conductivity,[18] and good homogeneity may improve the Li^+ diffusion in the cathode. Consequently, an improvement in the rate capability of p-$LiMn_{0.9}Cr_{0.1}O_2$ may be explained by two reasons. The first reason is the reduction in interparticle contact resistance due to the smaller particle size. The second reason is the increase of the diffusion efficiency of Li^+.

Conclusions

Layered $LiMn_{1-x}Cr_xO_2$ was synthesized by the Pechini method. With increasing EG content in the Pechini process, the homogeneity of layered $LiMn_{1-x}Cr_xO_2$ powder is increased, and the particle size is decreased. Compared with the ss-$LiMn_{1-x}Cr_xO_2$ powder, p-$LiMn_{1-x}Cr_xO_2$ compound yields a higher specific capacity for both charge and discharge, and the rate capability is improved due to the smaller particle size and good homogeneity. The evolution of discharge curves with cycling shows fewer additional spinel-type tetrahedral sites for Li intercalation/deintercalation during cycling for p-$LiMn_{1-x}Cr_xO_2$ compound. Therefore, the Pechini method could be a promising method for $LiMn_{1-x}Cr_xO_2$ compounds synthesis.

University of Wollongong assisted in meeting the publication costs of this article.

References

1. C. Sigala, A. Le Gal La Salle, Y. Piffard, and D. Guyomard, *J. Electrochem. Soc.*, **148**, A819 (2001).
2. M. M. Thackeray, W. I. F. David, P. G. Bruce, and J. B. Goodenough, *Mater. Res. Bull.*, **18**, 461 (1983).
3. M. M. Thackeray, R. A. De Kock, M. H. Rossouw, D. Liles, P. Bittihm, and D. Hoge, *J. Electrochem. Soc.*, **139**, 363 (1992).
4. R. Hoppe, G. Brachetel, and M. Jansen, *Z. Anorg. Allg. Chem.*, **471**, 1 (1975).
5. J. N. Reimers, E. W. Fuller, E. Rossen, and J. R. Dahn, *J. Electrochem. Soc.*, **140**, 3396 (1993).
6. R. J. Gummow, D. C. Liles, and M. M. Thackeray, *Mater. Res. Bull.*, **28**, 1249 (1993).
7. I. J. Davidson, R. J. McMillan, J. J. Murray, and J. E. Greedan, *J. Power Sources*, **54**, 232 (1995).
8. L. Croguennec, P. Deniard, and R. Brec, *J. Electrochem. Soc.*, **144**, 3323 (1997).
9. A. R. Armstrong and P. G. Bruce, *Nature (London)*, **381**, 499 (1996).
10. F. Capitaine, G. Gravereau, and C. Delmas, *Solid State Ionics*, **89**, 197 (1996).
11. C. Delmas and F. Capitaine, in Extended Abstracts of 8th International Meeting on Lithium Batteries, II-B-33, 470 (1996).
12. I. J. Davidson, R. S. McMillan, H. Slegr, B. Luan, I. Kargina, J. J. Murray, and I. P. Swainson, *J. Power Sources*, **81-82**, 406 (1999).
13. B. Ammundsen, J. Desilvestro, T. Groutso, D. Hassell, J. B. Metson, E. Regan, R. Steiner, and P. Pickering, *J. Electrochem. Soc.*, **147**, 4078 (2000).
14. V. Manov, A. Monchilov, A. Nassalevska, and A. Sato, *J. Power Sources*, **54**, 323 (1995).
15. W. Liu, G. C. Farrington, F. Chaput, and B. Cunn, *J. Electrochem. Soc.*, **143**, 879 (1996).
16. L. W. Tai and P. A. Lessing, *J. Mater. Res.*, **7**, 502 (1992).
17. A. Monchilov, V. Manev, and A. Nassalevska, *J. Power Sources*, **41**, 305 (1993).
18. J. Kim and A. Manthiram, *Electrochem. Solid-State Lett.*, **2**, 55 (1999).